Chemical Physics 177 (1993) 203–216
North-Holland

Triplet–triplet absorption of eosin Y in methanol determined by nanosecond excimer laser excitation and picosecond light continuum probing

A. Penzkofer and A. Beidoun
Naturwissenschaftliche Fakultät II – Physik, Universität Regensburg, D-93040 Regensburg, Germany

Received 19 April 1993

The absolute triplet–triplet absorption cross-section spectrum $\sigma_T(\lambda)$ of eosin Y in methanol at room temperature is determined in the wavelength region from 400 to 1000 nm and at 308 and 1054 nm. The triplet state is populated by XeCl excimer laser excitation to a singlet state and subsequent intersystem crossing. The triplet level population is determined by numerical simulation of the pump pulse absorption dynamics. The triplet–triplet absorption is probed with picosecond spectral light continua which are generated in a D_2O sample by a synchronized mode-locked Nd:glass laser. The decay of the triplet level population is studied by delayed picosecond light continua probing. Second order rate constants of $k_{ox}^{(1)} = 1.1\times10^9$ dm^3 mol^{-1} s^{-1} for oxygen quenching, $k_{TT}^{(1)} = 1.3\times10^9$ dm^3 mol^{-1} s^{-1} for triplet–triplet annihilation, and $k_{TS}^{(1)} = 4\times10^8$ dm^3 mol^{-1} s^{-1} for triplet–singlet concentration quenching have been determined.

1. Introduction

Eosin Y (the disodium salt of 2',4',5',7'-tetrabromofluorescein, structural formula is shown in fig. 12) has a high efficiency of triplet state formation by light excitation [1–3]. An enhanced intersystem crossing occurs due to the heavy atom effect of Br [2,4]. Phosphorescence [5] and delayed fluorescence [3,6–8] have been observed even at room temperature. Triplet excited eosin Y has a high efficiency of singlet oxygen generation [9–11] ($T+{}^3O_2 \rightarrow S+{}^1O_2$; T is eosin Y in triplet state and S is eosin Y in singlet state) and it acts as photosensitizer of chemical reactions [12,13] (photosensitized oxidation [14–18] and photosensitized reduction [19,20]).

The transfer of molecules to the triplet state changes the optical constants (refractive index and absorption coefficient) [21]. This behaviour led to applications in optical bistability [22], spatial light modulation [23] and all-optical switching [24]. The long triplet state lifetime allows low power long-pulse and cw ground-state absorption bleaching [21] leading to high nonlinear optical constants of slow response time [12,21,25] and finding applications in low power phase conjugation by four-wave mixing [26–32].

Efficient singlet–triplet intersystem crossing, population accumulation in the triplet state, and triplet–triplet absorption in the dye fluorescence region hinder long-pulse and cw pumped dye laser action [33–35], while laser action by short pulse pumping remains possible. Eosin Y laser action in various solvents was reported in refs. [36,37].

Triplet absorption data (peak extinction coefficients $\sigma_{T,max}$ and wavelength positions $\lambda_{T,max}$) are collected in refs. [38–40]. Absolute triplet–triplet absorption cross-section spectra $\sigma_T(\lambda)$ over wide wavelength regions are scarcely found [41–47]. Various methods for absolute triplet–triplet absorption cross-section determination have been invented and are reviewed in ref. [38] (energy transfer method [48], singlet depletion method [49], total depletion method [50], relative actinometry method [51], intensity variation method [52,53], kinetic method [54], partial saturation method [55], spatial separation of excitation and probing in fast flowing jet stream [47]).

Here we apply a nearly total depletion method to determine the absolute triplet–triplet absorption cross-section spectrum of eosin Y in methanol at room temperature. A powerful nanosecond XeCl excimer

laser is used to populate strongly the T_1 triplet level by singlet state excitation and subsequent intersystem crossing. The triplet–triplet absorption is probed by a time delayed picosecond spectral light continuum generated in a D_2O sample by mode-locked Nd:glass laser excitation. The applied technique allows the measurement of absolute triplet–triplet absorption cross-section spectra of dyes of high intersystem crossing rate ($k_{isc} \gtrsim 10^7\ s^{-1}$) even in the case of submicrosecond triplet-state lifetime (phosphorescence lifetime).

2. Theoretical considerations

A schematic energy level system of eosin Y including the pump pulse and probe pulse transitions is shown in fig. 1. The XeCl excimer laser (frequency ν_L) excites the molecules to a higher excited singlet state S_n (level 2) from where the molecules relax quickly to the lowest excited singlet state S_1 (level 3). Within the pump pulse duration Δt_L singlet excited-state absorption from level 3 to level 4 (S_m state) occurs. From the S_1 state the molecules relax to the triplet state T_1 (level 5) by intersystem crossing (k_{isc}) and to the S_0 ground state by radiative decay (τ_{rad}^{-1}) and internal conversion (k_{ic}). In the triplet manifold pump pulse attenuation occurs by triplet–triplet absorption (cross section $\sigma_{T,L}$) from level 5 to level 6. The lowest triplet level T_1 relaxes to the S_0 ground state with the phosphorescence time constant τ_P. A delayed picosecond spectral light continuum probes the triplet–triplet absorption (cross section $\sigma_T(\nu)$) from level 5 to higher triplet states (range 7).

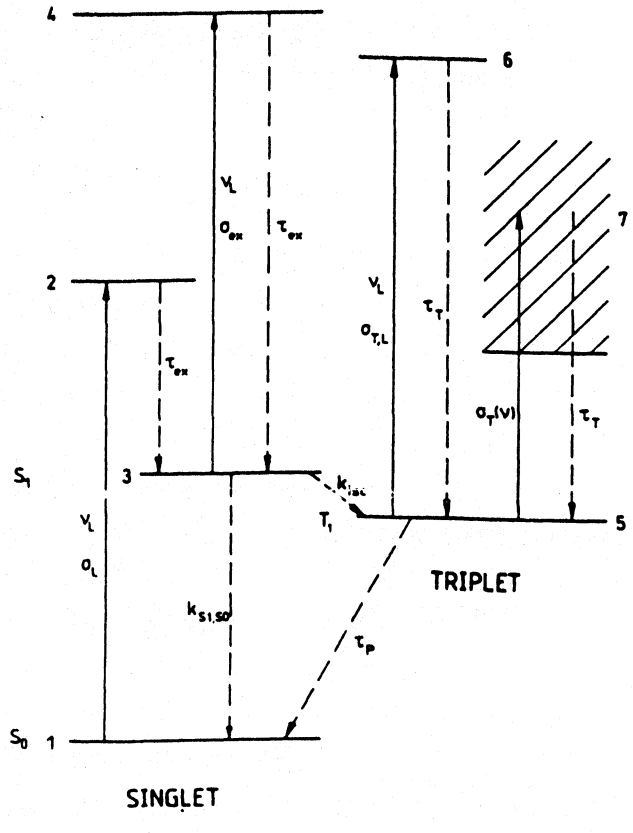

Fig. 1. Singlet and triplet level scheme of eosin Y. Transition with absorption cross sections, relaxation times and transition rates are indicated.

The pump pulse absorption dynamics is described by the following system of rate equations:

$$\frac{\partial N_1}{\partial t'} = -\frac{\sigma_L}{h\nu_L} N_1 I_L + k_{S_1,S_0} N_3 + \frac{N_5}{\tau_P}, \tag{1}$$

$$\frac{\partial N_3}{\partial t'} = \frac{\sigma_L}{h\nu_L} N_1 I_L - k_{S_1} N_3, \tag{2}$$

$$\frac{\partial N_5}{\partial t'} = k_{isc} N_3 - \frac{N_5}{\tau_P}, \tag{3}$$

$$\frac{\partial I_L}{\partial z'} = -(\sigma_L N_1 + \sigma_{ex} N_3 + \sigma_{T,L} N_5) I_L. \tag{4}$$

The moving frame transformation $t' = t - nz/c_0$ and $z' = z$ is used where t is the time, n is the refractive index, z is the coordinate along the propagation direction and c_0 is the light velocity in vacuum. The population number densities of the levels i are denoted by N_i. The relaxation time constants τ_{ex} [56] and τ_T [57] are very short (subpicosecond range) compared to the pump pulse duration ($\Delta t_L \approx 10$ ns). Therefore the level population number densities $N_2(t', z')$, $N_4(t', z')$, and $N_6(t', z')$ remain approximately zero over all times and do not appear in the above equation system (1)–(4). The S_1–S_0 relaxation rate k_{S_1,S_0} is given by $k_{S_1,S_0} = k_{ic} + \tau_{rad}^{-1}$, and the total S_1-state relaxation rate is $k_{S_1} = k_{S_1,S_0} + k_{isc} = \tau_F^{-1}$ where τ_F is the fluorescence lifetime. $I_L(t', z')$ is the pump pulse intensity at time t' and space coordinate z'. The phosphorescence lifetime τ_P is assumed to be constant in the description of the pump pulse absorption dynamics.

Eq. (4) describes isotropic absorption with orientationally averaged absorption cross sections σ_L, σ_{ex},

and $\sigma_{T,L}$. An isotropic treatment of the absorption dynamics is appropriate, because the orientational anisotropy caused by electric dipole interaction is averaged out on a nanosecond time scale ($\tau_{or} \ll \Delta t_L$) [58].

Amplification of spontaneous emission by stimulated emission (amplified spontaneous emission [58]) is not included in the equation system (for discussion see below).

The initial conditions of the level populations are $N_1(t'=-\infty,\ z)=N_0$ and $N_3(t'=-\infty,\ z')=N_5(t'=-\infty, z')=0$ where N_0 is the total dye number density. The temporal input pump pulse intensity distribution is approximated by a Gaussian profile, i.e.

$$I_L(t', z=0)=I_{0L}\exp[(-t'/t_L)^2]$$
$$=I_0\exp[-4\ln(2)t'^2/\Delta t_L^2],$$

where t_L is half the 1/e pulse width and Δt_L is the fwhm pulse duration. A rectangular profile was used for the spatial intensity distribution, which is a good approximation for apertured excimer laser pulses as applied in the experiments.

Eqs. (1)–(4) are solved numerically. The time integrated pump pulse transmission is given by

$$T_{TI}=\frac{w_L(l)}{w_L(0)}=\frac{\int_{-\infty}^{\infty} I_L(t', l)\,dt'}{\int_{-\infty}^{\infty} I_L(t', 0)\,dt'}, \tag{5}$$

where $w_L(0)$ and $w_L(l)$ are the energy densities of the pump pulses at the entrance and exit of the sample. The time-integrated transmission T_{TI} is identical to the energy transmission T_E because of the spatial rectangular intensity distribution. The unknown singlet excited-state absorption cross section σ_{ex} and the unknown triplet–triplet absorption cross section $\sigma_{T,L}$ at the pump laser frequency are determined by fitting the calculated T_{TI} curves to the experimental energy transmissions.

The temporal level populations $N_1(t', z)$, $N_3(t', z)$ and $N_5(t', z)$ are obtained by solving eqs. (1)–(4). They are averaged over the sample length by

$$\bar{N}_i(t')=\frac{1}{l}\int_0^l N_i(t', z)\,dz, \quad i=1, 3, 5. \tag{6}$$

The total number density of molecules in the triplet state manifold is denoted by N_T. N_T is practically equal to N_5 (fast relaxation of higher excited triplet states).

The dependences of the time-integrated transmissions T_{TI} and of the triplet level population N_T on pump pulse parameters and on singlet excited state absorption σ_{ex} and triplet–triplet absorption $\sigma_{T,L}$ are presented in figs. 2–7. The applied spectroscopic data of eosin Y are listed in table 1.

In fig. 2 the time-integrated pump pulse transmission is displayed versus input pump pulse peak intensity I_{0L} for $\sigma_{ex}=\sigma_{T,L}=0$. Curves are presented for various pulse durations. For $\Delta t_L < \tau_P$ the input peak intensity necessary for a certain absorption bleaching is roughly inversely proportional to the pulse duration. The medium behaves like a slow saturable absorber characterized by a saturation intensity of [59]

$$I_{sat,s}=\frac{h\nu_L}{\sigma_L\,\Delta t_L}. \tag{7}$$

For $\Delta t_L > \tau_P$ the input pulse peak intensity necessary for a certain energy density transmission becomes constant. The medium behaves like a fast saturable absorber with a saturation intensity of [58,59]

$$I_{sat,f,T}=\frac{h\nu_L}{\sigma_L\,\tau_P}. \tag{8a}$$

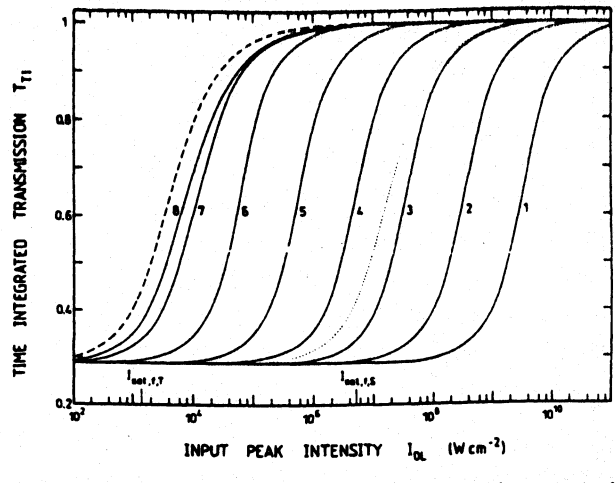

Fig. 2. Calculated dependence of time-integrated pump pulse transmission on input pump pulse peak intensity for various pulse durations. $N_0=2\times10^{16}$ cm^{-3}, $l=1$ cm, $\sigma_{ex}=\sigma_{T,L}=0$, $\tau_P=7.5$ μs. Input pulse durations are (1) $\Delta t_L=10$ ps, (2) 100 ps, (3) 1 ns, (4) 10 ns, (5) 100 ns, (6) 1 μs, (7) 10 μs, (8) 100 μs. Dashed curve, $k_{S_1,S_0}=0$ and $\Delta t_L=100$ μs (no S_1–S_0 relaxation). Dotted curve, $k_{isc}=0$ and $\Delta t_L=100$ μs (no triplet interaction). Other parameters are taken from table 1.

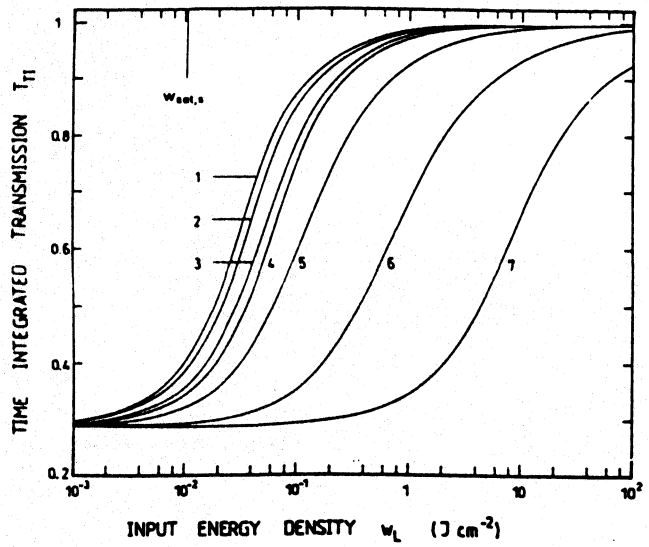

Fig. 3. Calculated dependence of time-integrated transmission on input pump pulse energy density for various pulse durations. $N_0=2\times10^{16}$ cm^{-3}, $l=1$ cm, $\sigma_{ex}=\sigma_{T,L}=0$, $\tau_P=7.5$ μs. Pulse durations are (1) $\Delta t_L=10$ ps, (2) 1 ns, (3) 10 ns, (4) 1 μs, (5) 10 μs, (6) 100 μs, (7) 1 ms.

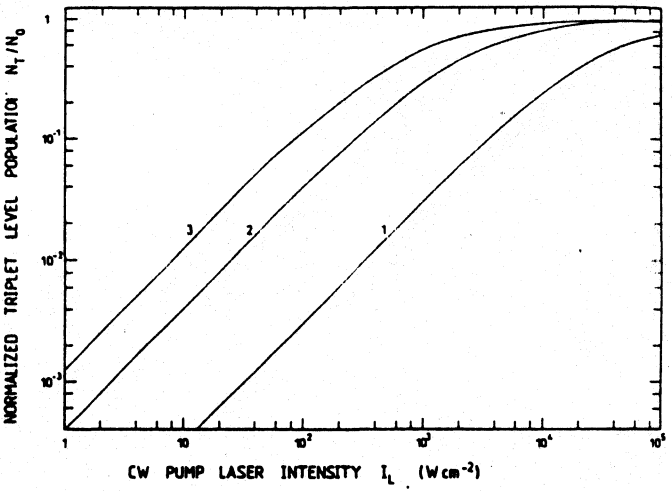

Fig. 5. Calculated dependence of normalized triplet level population number density $N_T(z)/N_0$ on laser intensity $I_L(z)$ under continuous pumping conditions. (1) $\tau_P=0.6$ μs, (2) $\tau_P=7.5$ μs, (3) $\tau_P=24$ μs. Other data are taken from table 1. For weak absorption ($T_0\to1$), $N_T(z)/N_0$ and $I_L(z)$ may be replaced by $\bar{N}_T/N_0$ and $I_L(0)$.

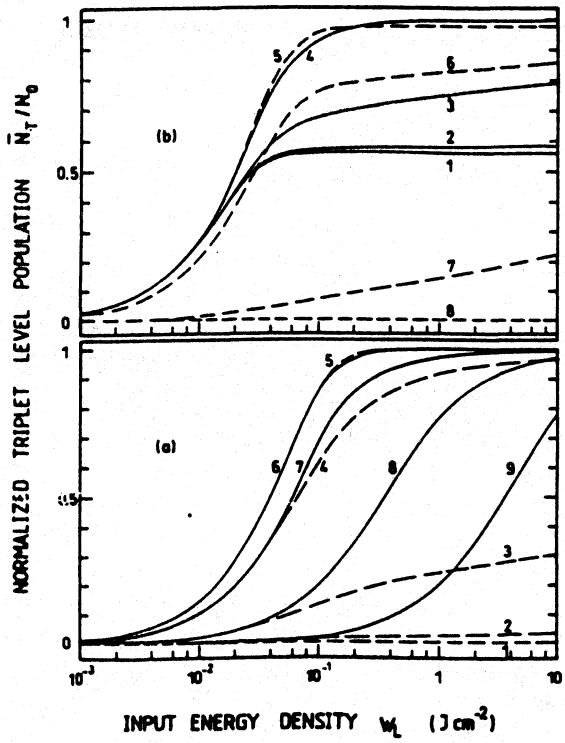

Fig. 4. Calculated dependence of sample-length averaged triplet level population $\bar{N}_T(t')$ on input pump pulse energy density. $N_0=2\times10^{16}$ cm^{-3}, $l=1$ cm, $\sigma_{ex}=\sigma_{T,L}=0$, $\tau_P=7.5$ μs. (a) $t'=0$ and (b) $t'=t_e=2\Delta t_L+5\tau_P$. The input pump pulse durations are (1) $\Delta t_L=10$ ps, (2) 100 ps, (3) 1 ns, (4) 10 ns, (5) 100 ns, (6) 1 μs, (7) 10 μs, (8) 100 μs, (9) 1 ms.

$I_{sat,f,T}$ is indicated by a vertical bar. The dashed curve is calculated for $k_{S_1,S_0}=0$ ($k_{S_1}=k_{isc}=5\times10^8$ s^{-1}) and $\Delta t_L=100$ μs. The partial S_1–S_0 relaxation requires a somewhat higher pump pulse intensity for bleaching (curve 8) than the situation of complete intersystem crossing (dashed curve). On the other hand the dotted curve is calculated for $k_{isc}=0$ ($k_{S_1}=k_{S_1,S_0}=5\times10^8$ s^{-1}) and $\Delta t_L=100$ μs. Considerably higher input pulse intensities are necessary for bleaching in this case of complete relaxation within the singlet system. The fast saturable absorber saturation intensity has increased to

$$I_{sat,f,S}=\frac{h\nu_L}{\sigma_1\tau_F}. \tag{8b}$$

The dependence of the time-integrated transmission on the input pulse energy density is depicted in fig. 3 for $\sigma_{ex}=\sigma_{T,L}=0$. The input pulse energy density necessary for a certain absorption bleaching is lowest and independent of pulse duration for $\Delta t_L<\tau_F$. It increases approximately by a factor of 2 by increasing the pulse duration from $\Delta t_L<\tau_F$ to $\Delta t_L\approx\tau_P$. In the case of $\Delta t_L>\tau_P$ the necessary input pulse energy for a fixed bleaching increases roughly linear with the pulse duration. In the case of $\Delta t_L<\tau_P$ (slow saturable absorption) the saturation energy density is [59]

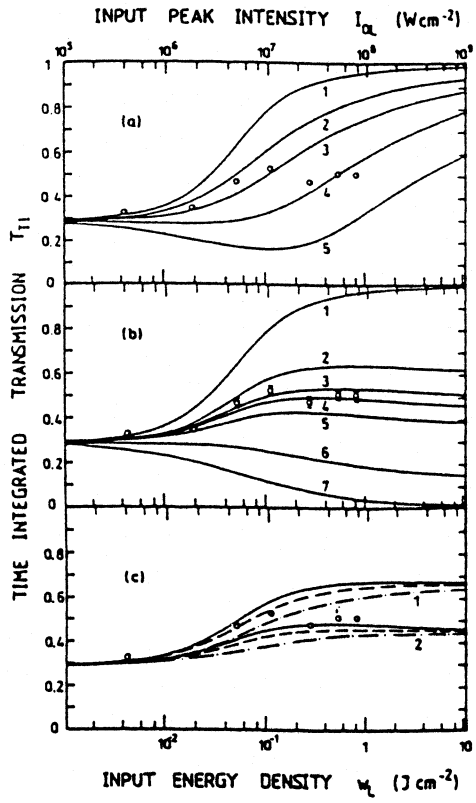

Fig. 6. Dependence of time-integrated transmission on input pump pulse energy density (lower abscissa) and on input pump pulse peak intensity (upper abscissa). $N_0=2\times10^{16}$ cm^{-3}, $l=1$ cm, $\Delta t_L=10$ ns. (a) Influence of singlet excited-state absorption σ_{ex}. $\sigma_{T,L}=0$. (1) $\sigma_{ex}=0$, (2) 5×10^{-17} cm^2, (3) 1×10^{-16} cm^2, (4) 2×10^{-16} cm^2, (5) 4×10^{-16} cm^2. (b) Influence of triplet–triplet absorption cross section $\sigma_{T,L}$. $\sigma_{ex}=0$. (1) $\sigma_{T,L}=0$, (2) 2.5×10^{-17} cm^2, (3) 3.5×10^{-17} cm^2, (4) 4×10^{-17} cm^2, (5) 5×10^{-17} cm^2, (6) 10^{-16} cm^2, (7) 2×10^{-16} cm^2. (c) Combined influence of σ_{ex} and $\sigma_{T,L}$. Solid curves, $\sigma_{ex}=1\times10^{-17}$ cm^2. Dashed curves, $\sigma_{ex}=2.5\times10^{-17}$ cm^2. Dash-dotted curves, $\sigma_{ex}=5\times10^{-17}$ cm^2. (1) $\sigma_{T,L}=2\times10^{-17}$ cm^2. (2) $\sigma_{T,L}=4\times10^{-17}$ cm^2. The curves are calculated and the circles are experimental data.

$$w_{sat,s}=\frac{h\nu_L}{\sigma_L}. \tag{9}$$

Its value is indicated by a vertical bar. For $\Delta t_L>\tau_P$ fast saturable absorption) the saturation energy density is given by

$$w_{sat,f}=\frac{h\nu_L}{\sigma_L\tau_P}\Delta t_L. \tag{10}$$

The triplet state population number density $\bar{N}_T(t')$ versus pump pulse energy density is shown in figs. 4a and 4b for $t'=0$ and $t'=t_e=2\Delta t_L+5\tau_F$, respectively. The curves apply to various pulse durations and $\sigma_{ex}=\sigma_{T,L}=0$. For $\Delta t_L<\tau_F$ the triplet level population

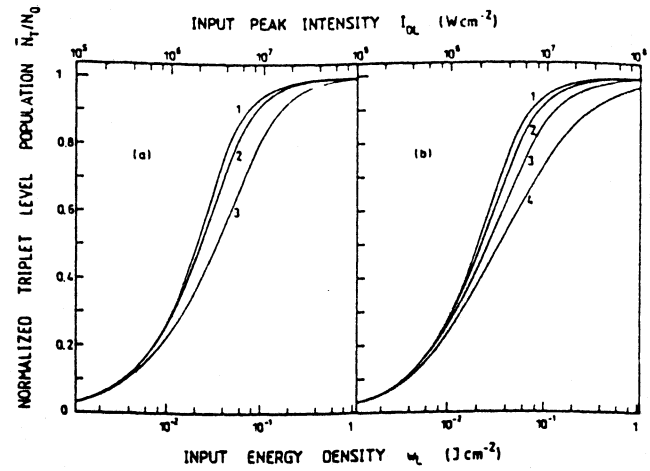

Fig. 7. Calculated dependence of sample length averaged triplet level population $\bar{N}_T(t_e)$ on input pump pulse energy density (lower abscissa) and on input pump pulse peak intensity (upper abscissa). $N_0=2\times10^{-16}$ cm^2, $l=1$ cm, $\Delta t_L=10$ ns. $t_e=30$ ns. (a) Influences of singlet excited-state absorption σ_{ex}. $\sigma_{T,L}=0$. (1) $\sigma_{ex}=0$, (2) 10^{-16} cm^2, (3) 4×10^{-16} cm^2. (b) Influence of triplet–triplet absorption cross section $\sigma_{T,L}$. $\sigma_{ex}=0$. (1) $\sigma_{T,L}=0$, (2) 4×10^{-17} cm^2, (3) 1×10^{-16} cm^2, (4) 2×10^{-16} cm^2.

continues to rise after the pump pulse has passed (curves 1–3), since the S_1-state level population continues to relax partly to the triplet state. The maximum triplet level population for very short pump pulses ($\Delta t_L\ll\tau_F$) is $N_{T,max}(t_e)=N_0k_{isc}/k_{S_1}=N_0\phi_T$ where ϕ_T is the quantum yield of triplet formation. For $\Delta t_L\gtrsim3k_{isc}^{-1}=3\tau_F/\phi_T$ practically complete accumulation of population in the triplet system is achievable. For $\Delta t_L\gtrsim\tau_P$ the triplet level population approaches a maximum around $t'=0$ (curves 7–9) and reduces towards the end of the pump pulse (triplet state relaxation to singlet ground state). The necessary pump pulse energy density for reaching a certain triplet level population becomes proportional to the pulse duration. The optimum pump pulse duration for efficient triplet level population at minimum pump pulse energy density is

$$\Delta t_{L,opt}=\min(3k_{isc}^{-1},\tau_P)=\min\left(\frac{3\tau_F}{\phi_T},\tau_P\right). \tag{11}$$

The spectroscopic data of eosin Y in methanol give $\Delta t_{L,opt}\approx10$ ns (see table 1).

Concerning cw pumping, the triplet level population is obtained from the system of equations (1)–(4) by setting the time derivatives of eqs. (1)–(3) equal to zero and using the relation $N_0=N_1+N_3+N_4$. The result is ($N_T=N_3$)

Table 1
Spectroscopic data of eosin Y in methanol at room temperature. Wavelength [illegible]

Parameter	Value	References
σ_L (cm^2)	6.2×10^{-17}	fig. 12
σ_{ex} (cm^2)	$<5\times10^{-18}$	fig. 6, this work
$\sigma_{T,L}$ (cm^2)	$(3.8\pm0.5)\times10^{-17}$	fig. 6, this work
τ_F (ns)	2	[57]
τ_{rad} (ns)	4.63	[57,85]
k_{S_1,S_0} (s^{-1})	2.2×10^8	[57]
k_{isc} (s^{-1})	2.8×10^8	[57]
ϕ_T	0.56	[57]
τ_{ex} (ps)	0.06	assumed, [56]
τ_T (ps)	1	[57]
$k_{ox}^{(1)}$ (dm^3 mol^{-1} s^{-1})	1.1×10^9	this work, [10] a)
$k_T^{(1)}$ (dm^3 mol^{-1} s^{-1})	1.3×10^9	this work, [71] a)
$k_S^{(1)}$ (dm^3 mol^{-1} s^{-1})	4×10^8	this work, [71] a)

a) Data for eosin Y in D_2O.

$$\frac{N_T}{N_0}=\frac{k_{isc}\tau_P I_L/I_{sat,f,S}}{1+(I_L/I_{sat,f,S})(1+k_{isc}\tau_P)}$$
$$=\frac{\Phi_T(\tau_P/\tau_F)I_L/I_{sat,f,S}}{1+(I_L/I_{sat,f,S})(1+\Phi_T\tau_P/\tau_F)}$$
$$=\frac{\phi_T\tau_P\sigma_L I_L/h\nu_L}{1+\sigma_L\tau_F I_L(1+\phi_T\tau_P/\tau_F)/h\nu_L}. \quad (12)$$

N_T/N_0 versus I_L is displayed in fig. 5 for eosin Y in methanol for three τ_P values. Eq. (12) shows that below saturation the steady-state triplet level population is proportional to $\phi_T\tau_P\sigma_L I_L$. High quantum yields of triplet formation, long phosphorescence lifetimes and large ground-state absorption cross sections are required to achieve reasonable triplet level population at moderate cw excitation intensity.

The influence of the singlet excited state absorption σ_{ex} on the time-integrated transmission T_{TI} is illustrated in fig. 6a for a pump pulse duration of $\Delta t_L=10$ ns and $\sigma_{T,L}=0$. The excited-state absorption reduces the absorption bleaching most effectively in an intermediate pump pulse energy density region. At high enough pump pulse energy densities a complete bleaching is approached because all molecules are transferred to the triplet state. The triplet state level population $\bar{N}_T(t_e=2\Delta t_L+5\tau_F)$ versus input pulse energy density w_L is displayed in fig. 7a for some σ_{ex} values. The fixed parameters are $\Delta t_L=10$ ns and $\sigma_{T,L}=0$. The singlet excited-state absorption lowers only slightly the rise of triplet level population with increasing input pump pulse energy density.

The dependence of T_{TI} on the triplet–triplet absorption cross section $\sigma_{T,L}$ is shown in fig. 6b for $\Delta t_L=10$ ns and $\sigma_{ex}=0$. A slight transmission maximum is obtained at an intermediate pump pulse energy density due to the nonabsorbing S_1-state level population within the pump pulse duration. For high pump pulse energy densities the transmission $T_{TI}(w_L\to\infty)\approx\exp(-N_0\sigma_{T,L}l)$ is approached since finally nearly all molecules are transferred to the triplet state ($\Delta t_L=10$ ns). The dependence of $\bar{N}_T(t_e)$ on $\sigma_{T,L}$ is shown in fig. 7b. There is a slight reduction of the rise of $\bar{N}_T(t_e, w_L)$ with growing $\sigma_{T,L}$.

The combined action of σ_{ex} and $\sigma_{T,L}$ on $T_{TI}(w_L)$ is illustrated in fig. 6c for three sets of σ_{ex} and $\sigma_{T,L}$ values. σ_{ex} reduced the transmission at intermediate energy densities. For $w_L\to\infty$ the triplet–triplet absorption limits the transmission to $T_{TI}(w_L\to\infty)\approx\exp(-N_0\sigma_{T,L}l)$.

The absorption of the spectral probe pulse continuum at time $t_d\geq t_e(N_3(t_d)=0)$ is given by

$$\frac{\partial w_{pr}(\nu)}{\partial z}$$
$$=-\{\sigma_S(\nu)[N_0-N_T(t_d)]+\sigma_T(\nu)N_T(t_d)\}$$
$$\times w_{pr}(\nu). \quad (13)$$

The spectrally resolved probe pulse transmission is

$$T_{pr}(\nu, t_d) = \frac{w_{pr}(\nu, l)}{w_{pr}(\nu, 0)}$$

$$= \exp\{-\sigma_S(\nu)[N_0 - \bar{N}_T(t_d)]l\} \times \exp[-\sigma_T(\nu)\bar{N}_T(t_d)l] \quad (14a)$$

$$= T_{pr,S}(\nu, t_d)\, T_{pr,T}(\nu, t_d) \quad (14b)$$

$$= T_0(\nu) \exp\{[\sigma_S(\nu) - \sigma_T(\nu)]\bar{N}_T(t_d)l\}, \quad (14c)$$

where $T_0(\nu) = \exp[-\sigma_S(\nu)N_0 l]$ is the small-signal ground-state transmission, $T_{pr,S}(\nu, t_d)$ is the probe pulse transmission due to S_0 ground-state population, and $T_{pr,T}(\nu, t_d)$ is the probe pulse transmission due to T_1 triplet level population. Solving eq. (14) to $\sigma_T(\nu)$ gives the triplet–triplet absorption cross-section spectrum

$$\sigma_T(\nu) = \frac{-\ln[T_{pr}(\nu, t_d)] - \sigma_S(\nu)[N_0 - \bar{N}_T(t_d)]l}{\bar{N}_T(t_d)l} \quad (15a)$$

$$= \frac{-\ln[T_{pr}(\nu, t_d)/T_{pr,S}(\nu, t_d)]}{\bar{N}_T(t_d)l} \quad (15b)$$

$$= \sigma_S(\nu) + \frac{\ln(T_0) - \ln[T_{pr}(\nu, t_d)]}{\bar{N}_T(t_d)l}. \quad (15c)$$

The triplet–triplet absorption cross-section spectrum is most accurately determined in the case of total singlet level depletion, i.e. $\bar{N}_T(t_d) = N_0$ (see eq. (13)) where $\sigma_T(\nu)$ reduces to $\sigma_T(\nu) = -\ln[T_{pr}(\nu, t_d)]/N_0 l$ (see eq. (15)). In our experiment the molecules are nearly completely transferred to the triplet system by the pump pulse (nearly total depletion method). In the nearly total depletion regime the method is insensitive to variations in pulse shape and pulse energy density.

In the analysis presented effects of amplification of spontaneous emission on the triplet level population have not been included. Amplified spontaneous emission shortens the S_1-state lifetime from τ_F to τ_{ASE} and thereby reduces the quantum yield of triplet formation ϕ_T from $k_{isc}\tau_F$ to $k_{isc}\tau_{ASE}$. The reduction of S_1-state lifetime by amplified spontaneous emission was derived in ref. [58]. It is given by

$$\frac{\tau_{ASE}}{\tau_F} \approx \left(1 + \frac{(\Delta\Omega/4\pi)\phi_F\sigma_{em}(\nu_{ASE})}{\sigma_{em}(\nu_{ASE}) - \sigma_{ex}(\nu_{ASE})} \times [\exp\{[\sigma_{em}(\nu_{ASE}) - \sigma_{ex}(\nu_{ASE})]N_3 l\} - 1]\right)^{-1}, \quad (16)$$

where ϕ_F is the fluorescence quantum yield, $\Delta\Omega = d_x d_y / l^2$ is the solid angle of effective amplified spontaneous emission ($d_x d_y = 2$ mm × 5 mm is the apertured beam size and $l = 1$ cm is the sample length in our experiments). $\sigma_{em}(\nu_{ASE})$ and $\sigma_{ex}(\nu_{ASE})$ are the stimulated emission cross section and the excited-state absorption cross section at the amplified spontaneous emission frequency ν_{ASE} (position of maximum gain), respectively. For our experimental situation ($\phi_F = 0.44$ [57], $N_0 = 2\times10^{16}$ cm^{-3}, $\sigma_{em}(\nu_{ASE}) \approx 2.7\times10^{-16}$ cm^2, $\sigma_{ex}(\nu_{ASE}) \approx 1.6\times10^{-17}$ cm^2, $\lambda_{ASE} \approx 550$ nm [60]) we estimate $1 > \tau_{ASE}/\tau_F \geq 0.96$ using $0 < N_3 \leq N_0/2$. Along the pump pulse duration, N_3 increases initially with the rise of the temporal Gaussian pump pulse intensity and then declines to zero due to intersystem crossing to the triplet system and relaxation to the singlet ground state. In our experiments the amplified spontaneous emission practically does not reduce the triplet level population and therefore does not influence the triplet–triplet absorption cross-section measurement.

3. Experimental

The experimental setup for the studies of the pump pulse excitation dynamics is shown in fig. 8a. A XeCl excimer laser (Lumonics type EX540, wavelength $\lambda_L = 308$ nm, maximum pulse energy 150 mJ, pulse duration $\Delta t_L \approx 10$ ns, maximum repetition rate 70 Hz, here operated in single shot mode) is used as excitation source. The laser pulse (flat-top profile of 8 mm × 30 mm cross section at laser exit, divergence 6 mrad × 1.5 mrad, temporal profile is approximately Gaussian) is focused by two crossed cylindrical lenses (focal length $f = 31$ cm). A central portion of constant energy density is selected by rectangular apertures A1 and A2 (1 mm × 3 mm). The time-integrated transmission through the dye sample S is measured by the photodetectors PD1 and PD2 (vacuum photocells of S20 spectral response). The input pulse energy is determined by the photodetector PD1 which

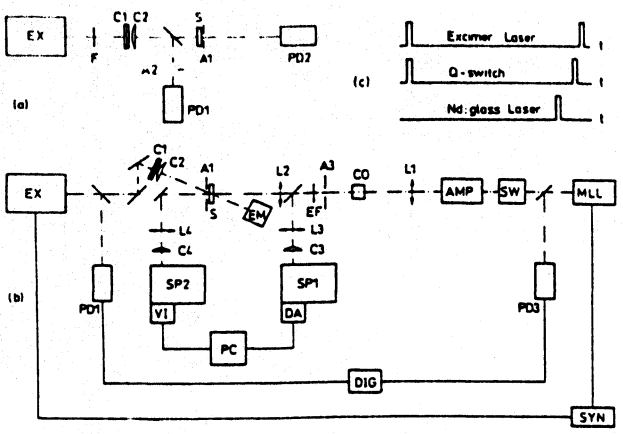

Fig. 8. Experimental setup for pump pulse absorption dynamics (a), triplet–triplet absorption spectrum measurement (b), and timing of excimer laser, Pockels cell Q-switch and mode-locked Nd:glass laser. EX, XeCl excimer laser. F, filter. C1–C4, cylindrical lenses. A1, A2, rectangular apertures. A3, circular aperture. S, eosin Y sample. PD1–PD3, photodetectors. EM, pyroelectric energy meter. EF, edge filter. CO, D_2O sample for light continuum generation. MLL, mode-locked Nd:glass laser. SW, Kerr cell shutter for single pulse selection. AMP, Nd:glass amplifier. SP1, SP2, 25 cm grating spectrometers. VI, vidicon system. DA, diode array system. PC, personal computer. DIG, transient digitizer. SYN, laser synchronization unit.

has been calibrated with a pyroelectric energy meter (Radiant dyes type PEM 50M). The input pump pulse energy to the sample is varied with glass plates F.

The experimental arrangement for the triplet–triplet absorption spectrum measurement is shown in fig. 8b. The dye molecules in the sample S (thickness 1 cm) are transferred to the triplet state by excitation with the excimer laser EX. A rectangular aperture A1 of size 2 mm × 5 mm in front of the sample cell selects a homogeneous energy density part out of the beam profile. The sample cell is tilted (angle ≈ 20°) to avoid amplification of fluorescence light reflected from the cell windows (avoiding of laser oscillation). The excitation pulse energy is measured with photodetector PD1. The transmission through the sample is determined by photodetector PD1 and pyroelectric energy meter EM. For the picosecond probe continuum generation an active (acousto-optic modulator IntraAction model ML-50Q) and passive (saturable absorber Kodak dye no. 9860 dissolved in 1,2-dichloroethane) mode-locked and Q-switched (Pockels cell Q-switch Gsänger model HVD1000) Nd:phosphate glass laser (wavelength 1.054 μm) [61] is applied in single shot operation mode. A single pulse is selected from the pulse train by a Kerr cell shutter [62] and increased in energy by passing through a Nd:phosphate glass amplifier. The generated single pulses have a duration of $\Delta t \approx 6$ ps and an energy of $W \approx 4$ mJ. These pulses are focused (lens L1, $f = 25$ cm) into a heavy water sample (cell CO, length $l = 5$ cm) in order to generate a picosecond light continuum [63–65]. Behind the heavy water cell the Nd:laser pulse is filtered off by an edge filter EF. The spectral continuum pulse is imaged to the dye sample S by lens L_2. Part of the input continuum is split off for detecting the input spectral energy distribution with a spectrometer SP1 and a diode array system DA. The transmitted spectral continuum is directed to a second spectrometer SP2 and a vidicon system VI. The spectral transmission is calculated from the ratio of output spectrum to input spectrum by a personal computer PC.

The excimer laser and the Nd:glass laser are temporally synchronized by a synchronization box SYN. The timing sequence of excimer laser charging (first pulse) and firing (second pulse, temporal separation ≈ 22 ms), Q-switch voltage on (first pulse) and Q-switch opening (second pulse), and Nd:glass laser flashlamp firing (approximately 550 μs before Q-switch opening) is displayed in fig. 8c. The timing between excimer laser pulse and Nd:glass laser pulse is adjusted by varying the time position of the Q-switch opening pulse with respect to the excimer laser firing pulse. The Nd:glass laser start pulse and the Q-switch opening pulse are locked to an adjustable time spacing. The time difference between Nd:glass laser pulse train and excimer laser pulse is measured by the photodetectors PD1 and PD3 and monitored on a transient digitizer DIG (Tektronix R7912). The timing jitter between excimer laser pulse and light continuum pulse was approximately ± 100 ns (could be reduced to ± 30 ns by operation of Nd:glass laser somewhat above laser threshold).

Eosin Y in methanol is investigated at room temperature. The dye was purchased from Heraeus and was purified by recrystallization six times from ethanol [20,66,67]. Methanol of analytic grade was purchased from Merck and used without further purification. For the triplet–triplet absorption cross-section measurements the dye solution was bubbled with nitrogen gas (purity 99.999 vol%) to outgas ox-

ygen [68–70] which quenches the triplet level population [66,68–71].

4. Results

The saturable absorption behaviour of eosin Y caused by excimer laser excitation is shown by the data points in fig. 6 (same points in parts a to c). Up to input energy densities of $w_L \approx 0.1$ J cm^{-2} the transmission rises with pump pulse energy density and then remains approximately constant. At high input pulse energy densities $w_L > 0.4$ J cm^{-2} some permanent dye decomposition was observed [71,72]. After about 20 shots with $w_L \approx 0.7$ J cm^{-2} the absorption coefficient at $\lambda_L = 308$ nm is reduced by approximately 5%.

The numerical fit to the experimental data (curves 3 and 4 in fig. 6b) gives a singlet excited-state absorption cross section of $\sigma_{ex} < 5 \times 10^{-18}$ cm^2 and a triplet–triplet absorption cross section of $\sigma_{T,L} = (3.8 \pm 0.5) \times 10^{-17}$ cm^2.

The spectral probe pulse transmission is shown by the solid curve in fig. 9. The displayed curve was obtained by spectrometer settings in the ranges 400 to 700 nm, 500 to 800 nm, and 700 to 1000 nm, and averaging over about five shots in each spectral range. The excimer pump laser energy density was kept constant at $w_L \approx 0.25$ J cm^{-2} resulting in a nearly complete transfer of eosin Y molecules to the triplet state ($\bar{N}_T(t_e = 30$ ns$)/N_0 = 0.97$, nearly total depletion method). The temporal delay of the probe pulse continuum with respect to the excimer laser pump pulse was in the region between 0.6 and 0.9 μs. The data point at $\lambda = 1054$ nm shows the transmission of the attenuated Nd:glass laser pulse through the sample at a delay time of $t_d \approx 0.75$ μs. The eosin Y sample was deaerated by nitrogen bubbling over a period of approximately twelve hours.

The dependence of the probe pulse transmission at $\lambda_{pr} = 580$ nm on the probe pulse delay $t_d - t_e$ is shown in fig. 10. The symbols indicate measured data and the curves are calculated (see below). The triangles were obtained without deaerating the eosin Y sample. A triplet state lifetime of $\tau_P = 0.6 \pm 0.2$ μs was obtained. The short triplet state lifetime is caused by oxygen quenching [20,66,68–71,73,74]. The dots were measured after about five hours of nitrogen bubbling through the sample. The decay of the curve

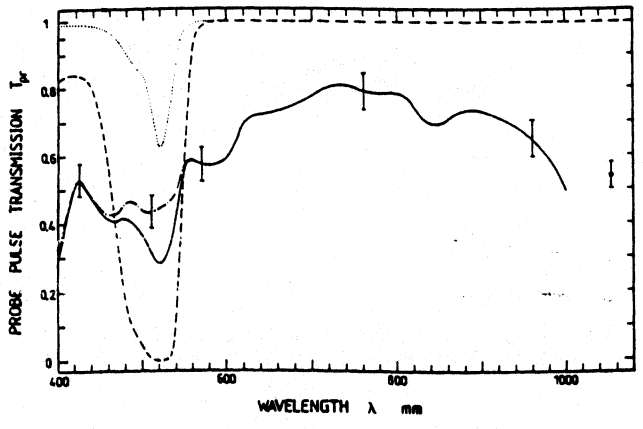

Fig. 9. Probe pulse transmission through eosin Y in methanol. $N_0 = 2 \times 10^{16}$ cm^{-3}, $l = 1$ cm. Solid curve, probe pulse transmission $T_{pr}(\lambda)$ at $t_d = 750 \pm 150$ ns and $w_L = 0.25$ J cm^{-2}. Dash-dotted curve, corrected probe transmission $T_{pr,T}$ considering only triplet–triplet absorption ($T_{pr,T} = T_{pr}/T_{pr,S}$, eq. (14b)). Dashed curve, ground-state transmission spectrum $T_0(\lambda) = \exp[-N_0\sigma_S(\lambda)l]$. Dotted curve, probe pulse transmission $T_{pr,S}$ caused by S_0 ground state population ($\bar{N}_1(t_d)/N_0 \cong 0.06$). Circle, probe pulse transmission at $\lambda = 1054$ nm (attenuated picosecond Nd:glass laser pulse).

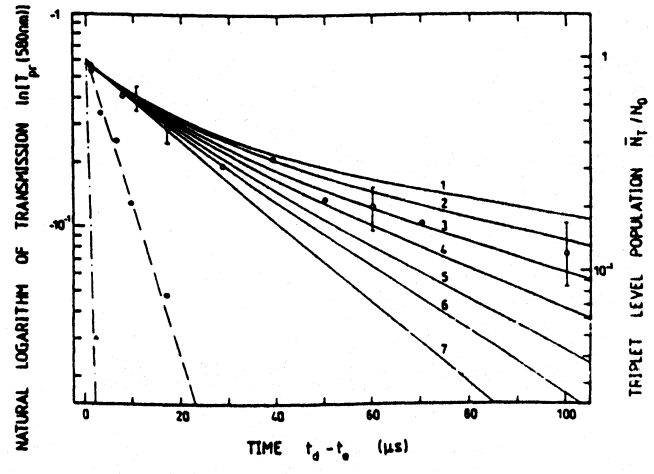

Fig. 10. Natural logarithm of probe pulse transmission, ln[T_{pr}(580 nm)] and triplet level population N_T versus probe pulse time position $t_d - t_e$ ($t_e = 30$ ns). $\bar{N}_T(t_e)/N_0 = 0.97$, $N_0 = 2 \times 10^{16}$ cm^{-3}, $l = 1$ cm (fig. 7b). Triangles and dash-dotted curve, air-saturated solution, $\tau_P = k_{ox}^{-1} = 0.6$ μs. Dots and dashed curve, nitrogen bubbling over a period of 5 h, $\tau_P = k_{ox}^{-1} = 7.5$ μs. Open circles, nitrogen bubbling over a period of 12 h. Solid curves are calculated for $k_{ox}^{(1)} = 0$, $k_{TT}^{(1)} = 1.3 \times 10^9$ dm^3 mol^{-1} s^{-1} and (1) $k_{TS}^{(1)} = 0$, (2) 2×10^8 dm^3 mol^{-1} s^{-1}, (3) 4×10^8 dm^3 mol^{-1} s^{-1}, (4) 6×10^8 dm^3 mol^{-1} s^{-1}, (5) 8×10^8 dm^3 mol^{-1} s^{-1}, (6) 1×10^9 dm^3 mol^{-1} s^{-1}, (7) 1.3×10^9 dm^3 mol^{-1} s^{-1}.

gives $\tau_P = 7.5 \pm 1.5$ μs. After about twelve hours of nitrogen bubbling the open circles were measured showing a non-exponential decay with an initial decay time of $\tau_P \approx 24$ μs and a decay time of $\tau_P \approx 60$ μs after about 70 μs. A discussion of the decay rates is given in the next section.

The temporal change of the probe pulse transmission at $\lambda_{pr} = 450$ nm is shown by the circles (measured values) and the solid curve (fitted through data points) in fig. 11. The temporal dependence is determined by the decay of triplet–triplet absorption, the build-up of ground-state singlet absorption and intermediate radical absorption. A discussion of the curve is given below.

5. Data analysis and discussion

The triplet level population $\bar{N}_T$ at the moment of probe pulse passing is calculated from the initial pump pulse population $\bar{N}_T(t_e)$ (curve 2 in fig. 7b). The temporal decay of $\bar{N}_T(t)$ is shown in fig. 10. For the solid transmission curve in fig. 9 a triplet population ratio of $\bar{N}_T$ (0.75 μs, 0.25 J cm^{-2})/$N_0 \approx 0.94$ is estimated ($\bar{N}_T(t_e)/N_0 \approx 0.97$ and curve 3 of fig. 10).

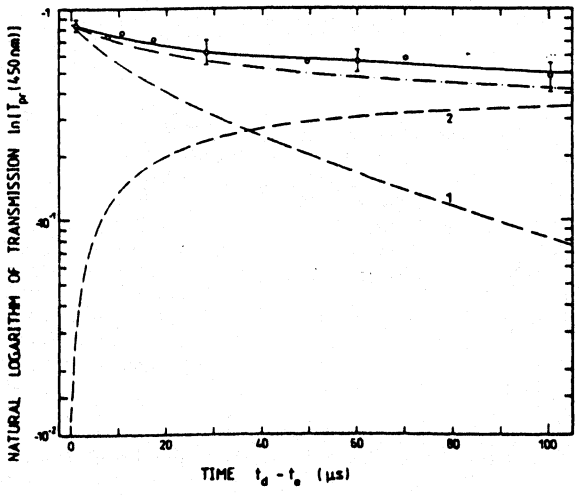

Fig. 11. Natural logarithm of probe pulse transmission, $\ln(T_{pr})$ at $\lambda_{pr} = 450$ nm versus probe pulse time position $t_d - t_e$ ($t_e = 30$ ns). $\bar{N}_T(t_e)/N_0 = 0.97$. $N_0 = 2 \times 10^{16}$ cm^{-3}, $l = 1$ cm. Circles, experimental points. Solid curve, fitted through experimental points. Dashed curve 1, $T_{pr,T}$ (contribution from triplet–triplet absorption); dashed curve 2, $T_{pr,S}$ (contribution from ground-state singlet absorption) assuming $N_1 = N_0 - N_T$ (no radical intermediates). Dash-dotted curve, $T_{pr,T} + T_{pr,S}$.

The initial ground-state transmission of the eosin Y sample before laser excitation is shown by the dashed curve in fig. 9. The residual ground-state absorption at the time of probe pulse passage is displayed by the dotted curve in fig. 9. It is calculated by

$$T_{pr,S}(t_d) = \exp\{-\sigma_s(\lambda)[N_0 - N_T(t_d)]l\}.$$

Knowing the singlet absorption contribution, the pure triplet–triplet emission is obtained by $T_{pr,T}(t_d) = T_{pr}(t_d)/T_{pr,S}(t_d)$ (eq. (14b)). The dash-dotted curve in fig. 9 shows $T_{pr,T}(t_d)$.

The triplet–triplet absorption cross-section spectrum $\sigma_T(\tilde{\nu})$ is given by $\sigma_T(\tilde{\nu}) = T_{pr,T}(t_d, \tilde{\nu})/\bar{N}_T(t_d)l$ (eq. (15b)). The solid curve in fig. 12 shows $\sigma_T(\tilde{\nu})$. The circle at 1054 nm belongs to the neodymium laser transmission measurement and the circle at 308 nm was obtained from the pump laser absorption bleaching measurements. The dashed curve shows the singlet ground-state absorption cross-section spectrum. The energy level positions of the S_1 state ($\tilde{\nu}_{S_1}$, from ref. [60]) and of the T_1 state ($\tilde{\nu}_{T_1}$, from refs. [73,75,76]) are indicated by vertical bars. The dash-dotted curve shows the shifted triplet–triplet absorption spectrum $\sigma_T(\tilde{\nu} - \tilde{\nu}_{S_1})$ for comparing with the S_0–S_n (S_n higher lying singlet states) absorption spectrum (dashed curve) (triplet–triplet absorption starts from $\tilde{\nu}_{T_1}$; singlet–singlet excited-state absorption starts from $\tilde{\nu}_{S_1}$). The triplet–triplet absorption cross-section spectrum is of the same order of magnitude as the S_1–S_n excited-state absorption cross-section spectrum [60]. Previously reported triplet–triplet absorption cross sections of eosin Y are listed in table 2. The data are in reasonable agreement with our measurements.

The depopulation of the triplet state [1–3,16,20,66,68–74] is caused by radiative decay (phosphorescence):

$$T_1 \xrightarrow{k_{P,rad}} S_0 + h\nu_P, \qquad (17)$$

by oxygen quenching:

$$T_1 + {}^3O_2 \xrightarrow{k_{ox}} S_0 + {}^1O_2, \qquad (18)$$

by triplet–triplet quenching (annihilation):

$$T_1 + T_1 \xrightarrow{k_{TT}} \begin{cases} \xrightarrow{k_{TTTS}} T_1 + S_0, & (19a) \\ \xrightarrow{k_{TTRX}} R + X \xrightarrow{k_{RXSS}} 2S_0, & (19b) \end{cases}$$

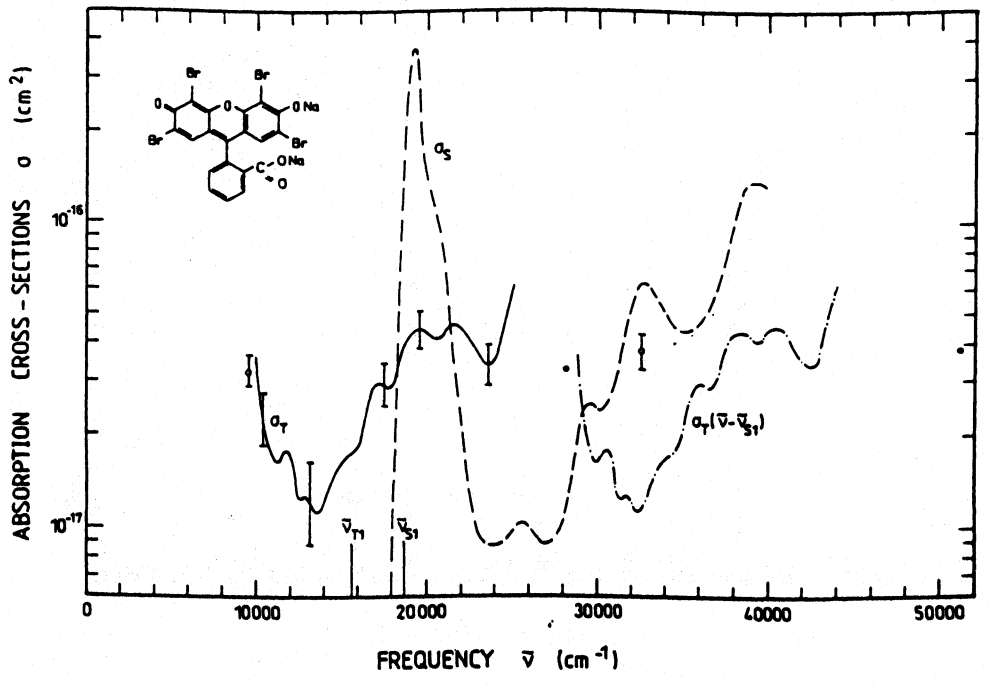

Fig. 12. Absorption cross-section spectra of eosin Y in methanol. Solid curve, $\sigma_T(\bar{\nu})$. Dashed curve, $\sigma_S(\bar{\nu})$. Dash-dotted curve, $\sigma_T(\bar{\nu}-\bar{\nu}_{S_1})$.

Table 2
Absolute triplet–triplet absorption cross sections of eosin Y

Solvent	Wavelength (nm)	σ_T (cm^2)	ϵ_T ($dm^3\,mol^{-1}\,cm^{-1}$)	Method	References
H_2O	590	3.18×10^{-17}	8315	FP	[69]
	625	2.94×10^{-17}	7685	FP	[69]
	580	3.12×10^{-17}	8150	FP	[71] [a]
	518	1.07×10^{-16}	2.2×10^4	FP	[86]
	527	5.5×10^{-17}	1.4×10^4	DPTA	[57]
ethanol	580	3.6×10^{-17}	9400	FP and SD	[87]
methanol	580	$(3\pm0.3)\times10^{-17}$	7850 ± 800	LFP	this work [a]
	527	4.9×10^{-17}	1.3×10^4	DPTA	[57]

[a] Spectra are shown. FP, flash photolysis. DPTA, double pulse transient absorption. LFP, laser flash photolysis. SD, singlet depletion. σ_T is absorption cross section derived from $T_T=\exp(-\sigma_T N_T l)$. ϵ_T is molar extinction coefficient derived from the optical density $D_T=-\log(T_T)=\epsilon_T C_T l$. The relation between σ_T in cm^2 and ϵ_T in $dm^3\,mol^{-1}\,cm^{-1}$ is $\epsilon_T=N_A\sigma_T/1000\ln(10)$ where $N_A=6.022045\times10^{23}$ mol^{-1} is the Avogadro constant.

and triplet–singlet quenching (concentration quenching):

$$T_1+S_0 \xrightarrow{k_{TS}} \begin{cases} \xrightarrow{k_{TSSS}} S_0+S_0, & (20a) \\ \xrightarrow{k_{TSRX}} R+X \xrightarrow{k_{RXSS}} 2S_0, & (20b) \end{cases}$$

where R is the semireduced radical of eosin Y [13,16,66,71] (an electron is added) and X is the semi-oxidized radical of eosin Y [13,16,66,71] (an electron is removed). $^3O_2$ is ground-state triplet oxygen and $^1O_2$ is excited singlet oxygen. The radicals R and X relax to singlet S_0 eosin Y. A first-order relaxation rate of $k_{RXSS}\approx0.75\times10^3\ s^{-1}$ was measured in the solvent ethanol [13].

The triplet quenching rates are

$$k_{ox} = k_{ox}^{(1)}[O_2] , \quad (21)$$

$$k_{TT} = k_{TTTS} + k_{TTRX} = k_{TT}^{(1)} C_T , \quad (22)$$

$$k_{TS} = k_{TSSS} + k_{TSRX} = k_{TS}^{(1)} C_S , \quad (23)$$

where $[O_2]$, C_T, and C_S are the oxygen, triplet eosin Y and singlet eosin Y concentrations, respectively.

The fast decay of triplet level population in the air-saturated eosin Y solution (triangles in fig. 10) is determined by oxygen quenching. The oxygen concentration is $[O_2] \approx 1.56\times10^{-3}$ mol/dm^3 [77]. The dash-dotted curve is calculated for $k_{ox}^{(1)} = 1.1\times10^9$ dm^3 mol^{-1} s^{-1} ($k_{ox} = 1.72\times10^6$ s^{-1}). This value was reported for eosin Y in water [16]. The dots in fig. 10 are still determined by oxygen quenching. From the decay rate of $k_{ox} = 1.3\times10^5$ s^{-1} (dashed curve) an oxygen concentration of $[O_2] = 2.1\times10^{-4}$ mol dm^{-3} is estimated.

The triplet level depopulation after twelve hours of N_2 bubbling is shown by the open circles in fig. 10. It is determined by triplet–triplet annihilation and by triplet–singlet quenching (concentration quenching). The relaxation dynamics is governed by

$$\frac{dC_T}{dt} = -[k_{TT}^{(1)} C_T + k_{TS}^{(1)}(C_0 - C_T)]C_T , \quad (24)$$

where C_0 is the total dye concentration ($C_S = C_0 - C_T$). In eq. (24) the radiative decay ($k_{P,rad}$), the oxygen quenching (k_{ox}, $[O_2] < 1.5\times10^{-5}$ mol dm^{-3}) and the semireduced and semi-oxidized radical formation and decay dynamics are neglected. The solution of eq. (24) (Bernoulli differential equation [78]) is

$$C_T(t_d) = C_T(t_e)\exp[-k_{TS}^{(1)} C_0(t_d - t_e)] \times\left(1 + \frac{k_{TT}^{(1)} - k_{TS}^{(1)}}{k_{TS}^{(1)}} \times\{1 - \exp[-k_{TS}^{(1)} C_0(t_d - t_e)]\}\frac{C_T(t_e)}{C_0}\right)^{-1} . \quad (25)$$

The solid curves in fig. 10 are calculated for $k_{TT}^{(1)} = 1.3\times10^9$ dm^3 mol^{-1} s^{-1} and various $k_{TS}^{(1)}$ values. The best fit to the experimental points gives $k_{TT}^{(1)} = (1.3\pm0.2)\times19^9$ dm^3 mol^{-1} s^{-1} and $k_{TS}^{(1)} = (4\pm2)\times10^8$ dm^3 mol^{-1} s^{-1}. The obtained values are in good agreement with reported data on $k_{TT}^{(1)}$ and $k_{TS}^{(1)}$ for eosin Y in H_2O [71].

The temporal transmission dependence at $\lambda = 450$ nm, shown by the circles and the solid curve in fig. 11, has contributions from triplet–triplet absorption (σ_T), ground-state singlet absorption (σ_S), and semi-oxidized radical absorption (σ_X) [66,68,71]. The dashed curve 1 shows the triplet–triplet transmission contribution $\ln[T_{pr,T}(450\text{ nm}, t_d)] = \ln[T_{pr,T}(450\text{ nm}, t_e)]\bar{N}_T(t_d)/\bar{N}_T(t_e)$. $T_{pr,T}(450\text{ nm}, t_d = 0.75\ \mu s) = 0.44$ is taken from fig. 9 and $\bar{N}_T(t_d)/\bar{N}_T(t_e)$ is displayed in fig. 10 (solid curve 3). The dashed curve 2 shows the ground-state singlet transmission contribution under the assumption of $C_S = C_0 - C_T$ (no semi-oxidized radical formation, $\ln[T_{pr,S}(450\text{ nm}, t_d)] = [N_0 - N_T(t_d)]\sigma_S(450\text{ nm})l$). The dash-dotted line represents the sum $\ln T_{pr,T} + \ln T_{pr,S}$. The difference $\ln T_{pr} - \ln T_{pr,T} - \ln T_{pr,S}$ gives an indication of semi-oxidized radical formation and radical absorption around 450 nm [66,68,71]. The absorption cross-section peak at 450 nm shown in fig. 12 may result from semi-oxidized radical absorption.

6. Conclusions

A laser flash photolysis technique [79–81] with excimer laser excitation source and picosecond light continuum monitoring source has been applied to determine the absolute triplet–triplet absorption cross-section spectrum $\sigma_T(\lambda)$ of eosin Y in methanol at room temperature in the wavelength region from 400 to 1000 nm. A XeCl excimer laser pulse of 10 ns duration transferred the molecules nearly completely to the lowest excited triplet state and a delayed picosecond spectral light continuum probed the triplet–triplet absorption. The lowest triplet level relaxation dynamics was monitored by varying the temporal delay of the probe pulse continuum. The tuning jitter between excimer laser pump pulse and light continuum probe pulse produced by a synchronized mode-locked Nd:glass laser could be reduced down to ±30 ns. Using short probe pulse delay times the described technique allows the measurement of triplet–triplet absorption cross-section spectra even for short phosphorescence lifetimes in the sub-microsecond range. The application of pump pulses of duration around 10 ns (excimer lasers [82] or Q-switched solid state lasers [83,84]) is most advantageous for molecules

with high intersystem crossing rates ($k_{isc} \gtrsim 10^8$ s^{-1}, $\phi_T \gtrsim 0.1$).

Acknowledgement

This work was supported by the Commission of the European Communities Directorate-General for Science, Research and Development in an international cooperation with the Technion – Israel Institute of Technology in Haifa (Professor Sh. Speiser). The authors are indebted to G. Gössl for building the laser synchronization unit. They thank the Rechenzentrum of the Universität Regensburg for allocation of computer time.

References

[1] C.A. Parker, Photoluminescence of solutions (Elsevier, Amsterdam, 1968).
[2] J.B. Birks, Photophysics of aromatic molecules (Wiley–Interscience, London, 1970).
[3] C.A. Parker, in: The triplet state, ed. A.B. Zahlan (Cambridge Univ. Press, Cambridge, 1967) p. 372.
[4] K.H. Drexhage, in: Topics in applied physics, Vol. 1. Dye lasers, ed. F.P. Schäfer, 3rd Ed. (Springer, Berlin, 1990) p. 155.
[5] Mlle. Boudin, J. Chem. Phys. 27 (1930) 285.
[6] C.A. Parker and C.G. Hatchard, Trans. Faraday Soc. 57 (1961) 1894.
[7] Yu.A. Soinikov, G.A. Ketsle and L.V. Levshin, J. Appl. Spectry. (USSR) 30 (1979) 309.
[8] G.A. Ketsle, L.V. Levshin and Yu.A. Soinikov, Opt. Spectry. (USSR) 52 (1982) 392.
[9] H.H. Wasserman and R.W. Murray, eds., Singlet oxygen (Academic Press, New York, 1979).
[10] A.P. Schaap, ed., Singlet molecular oxygen (Dowden, Hutchinson and Ross, Stroudsburg, PA, 1976).
[11] K. Gollnick and G.O. Schenck, Pure Appl. Chem. 9 (1964) 507.
[12] M. Koizumi, S. Kato, N. Magata, T. Matsuura and Y. Usui, Photosensitized reactions (Kagakudojin, Kyoto, 1978).
[13] M. Koizumi and Y. Usui, Mol. Photochem. 4 (1972) 57.
[14] P. Murasecco-Suardi, E. Gassmann, A.M. Braun and E. Oliveros, Helv. Chim. Acta 70 (1987) 1760.
[15] F. Amat-Guerri, M.M.C. López-González, R. Martinez-Utrilla and R. Sastre, Dyes Pigments 12 (1990) 249.
[16] V. Kasche, Photochem. Photobiol. 6 (1967) 643.
[17] E.F. Zwicker and L.I. Grossweiner, J. Phys. Chem. 67 (1963) 549.
[18] A.G. Kepka and L.I. Grossweiner, Photochem. Photobiol. 14 (1971) 621.
[19] A. Seret, E. Gandin and V. van de Vorst, J. Photochem. 38 (1987) 145.
[20] M. Nemoto, H. Kokubun and M. Koizumi, Bull. Chem. Soc. Japan 42 (1969) 1223.
[21] W.R. Tompkin, M.S. Malcuit and R.W. Boyd, Appl. Opt. 29 (1990) 3921.
[22] S. Speiser and F.L. Chisena, J. Chem. Phys. 89 (1988) 7259.
[23] S. Speiser and D. Dantsker, J. Appl. Phys. 66 (1989) 61.
[24] K.W. Beeson, J.T. Yardley and S. Speiser, Mol. Eng. 1 (1991) 1.
[25] M.A. Kramer, W.R. Tompkin and R.W. Boyd, Phys. Rev. A 34 (1986) 2026.
[26] Y. Silberberg and I. Bar-Joseph, Opt. Commun. 39 (1981) 265.
[27] I. Bar-Joseph, A. Hardy, Y. Katzir and Y. Silberberg, Opt. Letters 6 (1981) 414.
[28] I. Bar-Joseph and Y. Silberberg, Opt. Commun. 41 (1982) 455.
[29] K.P.B. Moosad, T.M. Abdul Rasheed and V.P.N. Namporri, Opt. Eng. 29 (1990) 47.
[30] K.P.B. Moosad, T.M. Adbul Rasheed, V.P.N. Namporri and K. Sathianandan, Appl. Opt. 29 (1990) 449.
[31] H. Fujiwara and K. Nakagawa, J. Opt. Soc. Am. B 4 (1987) 121.
[32] K. Nakagawa and H. Fujiwara, Opt. Commun. 70 (1989) 73.
[33] T.G. Pavlopoulos and P.R. Hammond, J. Am. Chem. Soc. 96 (1974) 6568.
[34] F.P. Schäfer, in: Topics in applied physics, Vol. 1. Dye lasers, ed. F.P. Schäfer, 3rd Ed. (Springer, Berlin, 1990).
[35] G. Jones II, in: Dye laser principles with applications, eds. F.J. Duarte and L.W. Hillman (Academic Press, New York, 1990).
[36] M. Maeda, Laser dyes (Academic Press, London, 1984) p. 101.
[37] A.V. Deshpande and N.B. Iyer, J. Luminescence 46 (1990) 339.
[38] I. Carmichael and G.L. Hug, J. Phys. Chem. Ref. Data 15 (1986) 1.
[39] I. Carmichael, W.P. Helman and G.L. Hug, J. Phys. Chem. Ref. Data 16 (1987) 239.
[40] I. Carmichael and G.L. Hug, in: Handbook of organic photochemistry, Vol. 1, ed. J.C. Scaiano (CRC Press, Boca Raton, 1989) p. 369.
[41] R. Astier and Y.H. Meyer, in: The triplet state, ed. A.B. Zahlan (Cambridge Univ. Press, 1967) p. 447.
[42] D.N. Dempster, T. Morrow and M.F. Quinn, J. Photochem. 2 (1973/74) 403.
[43] T.G. Pavlopoulos, Spectrochim. Acta A 42 (1986) 47.
[44] T.G. Pavlopoulos, Proc. Soc. Photo-Opt. Instrum. Eng. 1437 (1991) 168.
[45] T.G. Pavlopoulos and D.J. Golich, J. Appl. Phys. 67 (1990) 1203.
[46] T.G. Pavlopoulos, J.H. Boyer, K. Thangaraj, G. Sathyamoorthi, M.P. Shah and M.L. Soong, Appl. Opt. 31 (1992) 7089.

[47] E. Thiel and K.H. Drexhage, Chem. Phys. Letters 199 (1992) 329.
[48] R. Bensasson and E.J. Land, in: Photochemical and photobiological reviews, Vol. 3, ed. K.C. Smith (Plenum Press, New York, 1978) p. 163.
[49] S.G. Hadley and R.A. Keller, J. Phys. Chem. 73 (1969) 4351.
[50] G. Porter and M.W. Windsor, J. Chem. Phys. 21 (1953) 2088.
[51] H. Lutz, E. Breheret and L. Lindqvist, J. Phys. Chem. 77 (1973) 1758.
[52] D.S. McClure, J. Chem. Phys. 19 (1951) 670.
[53] T.G. Pavlopoulos, Spectrochim. Acta A 43 (1987) 1201.
[54] D. Lavalette, Compt. Rend., Acad. Sci. B 266 (1968) 279.
[55] U. Lachish, A. Shafferman and G. Stein, J. Chem. Phys. 64 (1976) 4205.
[56] F. Graf and A. Penzkofer, Opt. Quantum Electron. 17 (1985) 53.
[57] A. Penzkofer, A. Beidoun and M. Daiber, J. Luminescence 51 (1992) 297.
[58] A. Penzkofer and W. Blau, Opt. Quantum Electron. 15 (1983) 325.
[59] A. Penzkofer and W. Bäumler, Opt. Quantum Electron. 23 (1991) 727.
[60] A. Penzkofer, A. Beidoun and S. Speiser, Chem. Phys. 170 (1993) 139.
[61] W. Scheidler and A. Penzkofer, Opt. Commun. 80 (1990) 127.
[62] D. von der Linde, O. Bernecker and A. Laubereau, Opt. Commun. 2 (1970) 215.
[63] A. Penzkofer and W. Kaiser, Opt. Quantum Electron. 9 (1977) 313.
[64] A. Penzkofer, A. Beidoun and H.J. Lehmeier, Opt. Quantum Electron. 25 (1993) 317.
[65] R.R. Alfano, ed., The supercontinuum laser source (Springer, New York, 1989).
[66] T. Ohno, S. Kato and M. Koizumi, Bull. Chem. Soc. Japan 39 (1966) 232.
[67] G. Jones II and S. Chatterjee, J. Phys. Chem. 92 (1988) 6862.
[68] G.J. Fisher, C. Lewis and D. Madill, Photochem. Photobiol. 24 (1976) 223.
[69] A. Seret, E. Gandin and A. van de Vorst, Chem. Phys. Letters 135 (1987) 427.
[70] A. Seret and A. van de Vorst, J. Phys. Chem. 94 (1990) 5293.
[71] V. Kasche and L. Lindqvist, Photochem. Photobiol. 4 (1965) 923.
[72] K. Uchida, S. Kato and M. Koizumi, Nature 184 (1959) 1620.
[73] V.E. Korobov and A.K. Chibisov, Russ. Chem. Rev. 52 (1983) 27.
[74] I. Kraljic and L. Lindqvist, Photochem. Photobiol. 14 (1974) 621.
[75] N.I. Kunavin, R.N. Nurmukhametov and T.G. Khachaturova, J. Appl. Spectry. (USSR) 26 (1977) 735.
[76] R.W. Chambers and D.R. Kearns, Photochem. Photobiol. 10 (1969) 215.
[77] A. Kruis and A. May, in: Landolt-Börnstein, Zahlenwerte und Tabellen aus Physik, Chemie, Geophysik und Technik. 6. Edition, Band II. Eigenschaften der Materie in ihrer Aggregatzuständen. 2. Teil, Bandteil B, Lösungsgleichgewichte I, eds. K. Schäfer and E. Lax (Springer, Berlin, 1962) p. 178.
[78] I.N. Bronstein and K.A. Semendjajev, Taschenbuch der Mathematik, 22nd Ed. (Deutsch, Thun, 1985) p. 421.
[79] G. Porter and M.A. West, in: Techniques of chemistry, Vol. VI B, ed. G.G. Hammes (Wiley–Interscience, New York, 1974) p. 367.
[80] C. Scaiano, Accounts Chem. Res. 16 (1983) 234.
[81] L.M. Hadel, in: CRC handbook of organic photochemistry, Vol. I, ed. J.C. Scaiano (CRC Press, Boca Raton, 1989) p. 279.
[82] Ch.K. Rhodes, ed. Topics in applied physics, Vol. 30. Excimer lasers (Springer, Berlin, 1984).
[83] A. Penzkofer, Prog. Quantum Electron. 12 (1988) 291.
[84] W. Koechner, Solid state laser engineering, 3rd Ed. (Springer, Berlin, 1992).
[85] K. Gollnick, in: Advances in photochemistry, Vol. 6, eds. W.A. Noyes Jr., G.S. Hammond and J.N. Pitts Jr. (Wiley–Interscience, New York, 1968) p. 2.
[86] P.G. Bowers and G. Porter, Proc. Roy. Soc. A 299 (1967) 348.
[87] K. Kikuchi, H. Kokuban and M. Koizumi, Bull. Chem. Soc. Japan 44 (1971) 1527.